Pt Nanoparticle Binding on Functionalized Multiwalled Carbon Nanotubes

Robert V. Hull,[†] Liang Li,[‡] Yangchuan Xing,[‡] and Charles C. Chusuei*,[†]

Departments of Chemistry and Chemical and Biological Engineering, University of Missouri−Rolla, Rolla, Missouri 65409-0010

Received August 23, 2005. Revised Manuscript Received January 14, 2006

To create new catalyst materials for fuel cell applications, multiwalled carbon nanotubes (CNTs) were functionalized with −C═O, −C−O−C−, −COO−, and −C−OH groups using a sonochemical treatment method under acidic aqueous solution (HNO_3/H_2SO_4) conditions to make them amenable to deposition of highly dispersed, ∼4 nm diameter Pt nanoparticles. The Pt−CNT interface was probed with X-ray photoelectron spectroscopy (XPS), extended X-ray absorption fine structure spectroscopy (EXAFS), and Raman and attenuated total reflection infrared (ATR-IR) spectroscopies to elucidate the nature of the Pt cluster−CNT surface binding. The degree of disorder of the sp^3-hybridized C from the CNTs, as measured by the Raman D-to-G integrated peak area ratios, increased with the degree of surface oxidation of the CNTs. EXAFS of the Pt L_{III} edge showed Pt coordination with oxygen (in the form of PtO_x) at the outermost perimeter of the Pt clusters while the majority of the bulk, as shown by the XPS Pt 4f core level, was in the metallic form. Infrared measurements showed that the carbonyl C═O stretching at 1700 cm^{-1} red shifted to ∼1550 cm^{-1} following Pt cluster deposition. In addition, changes in the C−O structural features at ∼1030 and 1150 cm^{-1} were observed, indicative of Pt cluster binding with the ionic form of carboxylate, COO(Pt), or ester-like, C(═O)CO(Pt), O atoms.

Introduction

Fuel cells are electrochemical devices with a constant replenishment of reactants as "fuel", which are promising as clean, renewable sources of energy. In this process, electrical energy is generated by chemically combining two reactants at a solid catalyst interface between the chemical cells. Because noble metals are typically used as the catalysts, a maximum in catalytic power corresponding to a minimal mass of catalyst is highly desirable for reduced cost in their design. Carbon nanotubes (CNTs), due to their special electronic[1] and mechanical[2] properties, have been found to be useful as heterogeneous catalyst supports[3−9] and readily applied for Pt nanoparticle deposition. Initial studies by Li et al.[7] have shown that Pt supported on CNTs produced a greater power density than when supported on carbon black in the oxygen reduction reaction (ORR) of direct methanol fuel cells (DMFC). Moreover, we further increased the electrocatalytic activity by 48% relative to carbon black using sonication to pretreat the CNTs.[10,11] The reasons underlying the improved performance are not well-understood but are likely related to the Pt−CNT interfacial structure. There is a paucity of surface structural information to explain reasons underlying the optimum nanoparticle dispersion and avoidance of agglomeration. The nature of the CNT−Pt cluster binding in terms of the participation of the various types of oxygen species has not been well elucidated and is the focus of this current study. Investigation of these Pt loaded surfaces may lead to a better understanding of factors governing Pt−CNT stability and leading to improved ORR activity.

Experimental Section

Multiwalled CNTs were obtained from Nanolab, Inc. (95% purity), and functionalized using a sonochemical treatment method developed in our laboratory.[10,11] This procedure rapidly and effectively oxidizes the CNTs after a 2-h treatment, allowing for deposition of finely dispersed Pt nanoparticles while avoiding admetal aggregation. Attempts at producing Pt nanoparticles tethered to the 1- and 8-h treated surfaces were not successful as oxidation of the surface groups at these conditions hampered the nanoparticle deposition (vide infra). Pt was successfully deposited onto the 2- and 4-h treated surfaces as finely dispersed nanopar-

* To whom correspondence should be addressed. E-mail: chusuei@umr.edu. Tel.: 573-341-4537. Fax: 573-341-6033.
[†] Department of Chemistry.
[‡] Department of Chemical and Biological Engineering.

(1) Odom, T. W.; Huang, J.-L.; Kim, P.; Lieber, C. M. *Nature* **1998**, *391*, 62−64.
(2) Falvo, M. R.; Clary, G. J.; Taylor, R. M., II; Chi, V.; Brooks, J. F. P.; Washburn, S.; Superfine, R. *Nature* **1997**, *389*, 582−584.
(3) Planeix, J. M.; Coustel, N.; Coq, B.; Brotons, V.; Kamblar, P. S.; Dutartre, R.; Geneste, P.; Bernier, P.; Ajayan, P. M. *J. Am. Chem. Soc.* **1994**, *116*, 7935−7936.
(4) Freemantle, M. *Chem. Eng. News* **1996**, *74*, 62.
(5) Che, G.; Lakshmi, B. B.; Fisher, E. R.; Martin, C. R. *Nature* **1998**, *393*, 346−349.
(6) Che, G.; Lakshmi, B. B.; Martin, C. R.; Fisher, E. R. *Langmuir* **1999**, *15*, 750−758.
(7) Li, W.; Liang, C.; Qiu, J.; Zhou, W.; Han, H.; Wei, Z.; Sun, G.; Xin, Q. *Carbon* **2002**, *40*, 791−794.
(8) Yoshitake, T.; Shimakawa, S.; Kimura, H.; Ichihashi, T.; Kubo, Y.; Kasuya, D.; Yakahashi, K.; Kokai, F.; Yudasaka, M.; Iijima, S. *Physica B* **2002**, *323*, 124−126.
(9) Gennett, T.; Landi, B. J.; Elich, J. M.; Jones, K. M.; Alleman, J. L.; Lamarre, P.; Morris, R. S.; Raffaelle, R. P.; Heben, M. J. *Mater. Res. Soc. Symp. Proc.* **2003**, *756*, 379−384.
(10) Xing, Y. *J. Phys. Chem. B* **2004**, *108*, 19255−19259.
(11) Xing, Y.; Li, L.; Chusuei, C. C.; Hull, R. V. *Langmuir* **2005**, *21*, 4185−4190.

10.1021/cm0518978 CCC: $33.50
Published on Web 03/09/2006

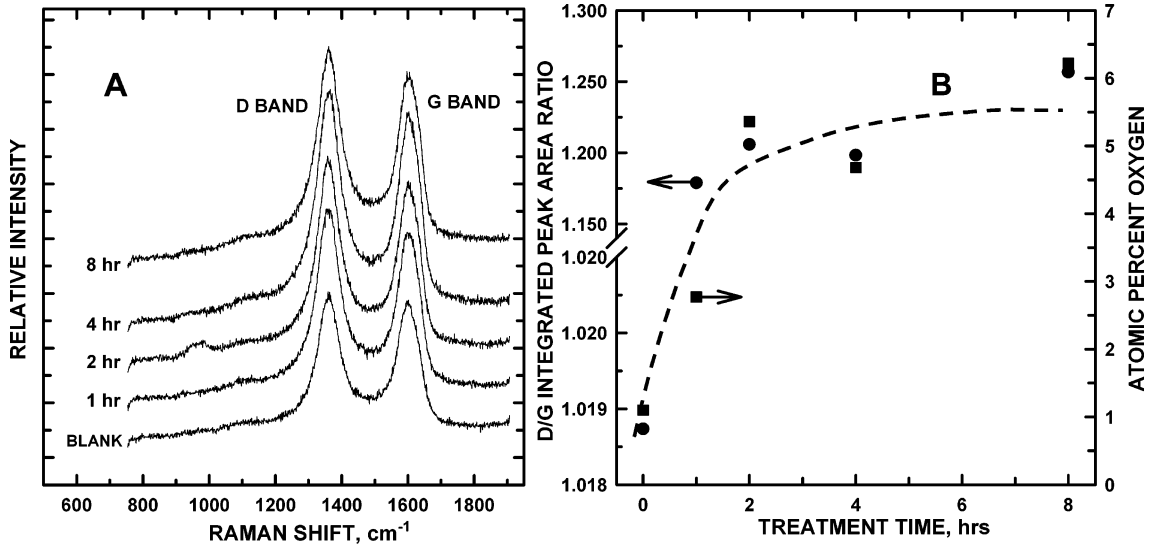

Figure 1. (A) Raman shifts showing the emergence of the D and G bands of sonochemically treated CNTs before deposition of Pt nanoparticles. Raw data are shown. (B) A plot of the uptake of D-to-G integrated peak area ratios (●, left-hand axis) and atomic percent oxygen from ref 13 (■, right-hand axis) versus sonochemical treatment time. The dashed line serves as a guide to the eye, denoting functional group saturation at ∼2 h.

ticles. For the purposes of this study, we focused on 20 wt % Pt loadings on the 2-h sonicated CNTs because this produced the optimum Pt−CNT surface both in terms of the quality of the dispersion and short preparation time. CNTs without deposited Pt and 4-h sonochemically treated surfaces with a 20 wt % Pt loading were examined for comparison.

The integrity of the oxidized CNTs with and without the Pt clusters was examined with a Triax 320 Raman spectrometer, equipped with a confocal microscope, a liquid N_2 cooled Ge detector, and an Ar ion laser ($\lambda = 514.4$ nm) to probe the sp^2- (ordered) and sp^3- (disordered) hybridized C peaks. Raman samples were prepared by dropping aliquots of the sonochemically treated CNTs (with and without the Pt clusters from the colloidal aqueous solutions) onto Si(100) 1 cm × 1 cm substrates and drying in air. To verify that Pt nanoparticles were formed on the surface, transmission electron microscopy (TEM) micrographs were obtained using an EM430 Philips electron microscope operating at 300 kV. A small quantity of the Pt nanoparticles supported on the CNTs (Pt−CNT) was dispersed in ethanol, of which a drop was then deposited on a 400 mesh carbon-coated Cu TEM grid (Electron Microscopy Sciences) which was then allowed to dry prior to imaging. A total of 450−500 nanoparticles were counted to ensure a statistically representative sampling. X-ray photoelectron spectroscopy (XPS) elemental binding energy (BE) and integrated peak area measurements were made using a Kratos 165 XP spectrometer equipped with a hemispherical analyzer and Mg Kα anode ($h\nu =$ 1253.6 eV). High-resolution scans of the Pt 4f level were performed at a 20 eV pass energy.

Further structural analysis was performed using extended X-ray absorption fine structure (EXAFS). Spectra were obtained from the 12-BM BESSRC Advanced Photon Source (APS) beamline at the Argonne National Laboratory and the X18B beamline at the National Synchrotron Light Source (NSLS) at the Brookhaven National Laboratory to analyze the Pt L_{III} edge (11.564 keV) of the Pt nanoparticles tethered to the CNT surface. Although all of the spectra could have been obtained at either facility, due to limited beamtime access both were used to acquire the data. A spectrum of a 5 μm thick Pt foil was taken in the transmission mode for absolute energy calibration. The absorption edge of the data obtained for each sample, plotted as $\chi(E)$, was checked to ensure alignment prior to plotting in k space. Spectra of the dried Pt/CNT samples and PtO_2 standard (obtained in fluorescence mode) were obtained at the APS while those of the aqueous solution Pt/CNT were obtained at the NSLS. Anhydrous PtO_2 (99.95% purity, metals basis) obtained from Alfa Aesar, 8 mg of which were diluted in 170 mg BN, was used for the reference spectrum. In both beamlines, a double crystal Si(111) monochromator was used for energy selection. Spectra taken in the fluorescence mode used a 13-element Ge detector. The ion chambers employed had a 8:2 gas mixture of N_2-to-Ar. Data were processed using the IFEFFIT library of numerical XAS algorithms written in Perl programming that utilizes the ab initio EXAFS code, FEFF 6.01.[12,13]

Surface vibrational data were obtained using a Nicolet Nexus 470 Fourier transform infrared spectrometer having a resolution of 4 cm^{-1}. A horizontal attenuated total reflection infrared (ATR-IR) solid powder holder, consisting of a ZnSe crystal, was incorporated into the sample compartment to analyze the functionalized and Pt cluster deposited CNTs. The Pt−CNTs were pipetted onto the ZnSe surface and allowed to dry prior to scans. To exclude spectral artifacts from H_2O and atmospheric CO_2 contamination in the ATR-IR experiments, the sample was purged with N_2 gas (99.9% purity) for 30 min prior to and during IR data collection. The infrared data was processed using OMNI-C, version 5.0 (Nicolet Instrument Corp.), software. The signals from the untreated CNTs were used as blanks for obtaining the infrared difference spectra.

Results and Discussion

The Raman stackplot (Figure 1A) of the sonochemically treated CNTs show D and G bands at 1352 and 1596 cm^{-1} corresponding to the sp^3- and sp^2-hybridized carbons signifying disordered graphite and the ordered state on the CNT surface, respectively.[14,15] Upon deposition of the Pt nanoparticles, the Raman line shapes and relative D-to-G band intensities (not shown) remained unchanged. The presence of these peaks verified that the CNTs remained largely intact during the oxidation procedure and after deposition of the

(12) Newville, M. *J. Synchrotron Radiat.* **2001**, *8*, 322−324.
(13) Ravel, B.; Newville, M. *J. Synchrotron Radiat.* **2005**, *12*, 537−541.
(14) Dresselhaus, M. S.; Dresselhaus, G.; Jorio, A.; Souza Filho, A. G.; Saito, R. *Carbon* **2002**, *40*, 2043−2061.
(15) Martinez, M. T.; Callejas, M. A.; Benito, A. M.; Cochet, M.; Seeger, T.; Anson, A.; Schreiber, J.; Gordon, C.; Marhic, C.; Chauvet, O.; Fierro, J. L. G.; Maser, W. K. *Carbon* **2003**, *41*, 2247−2256.

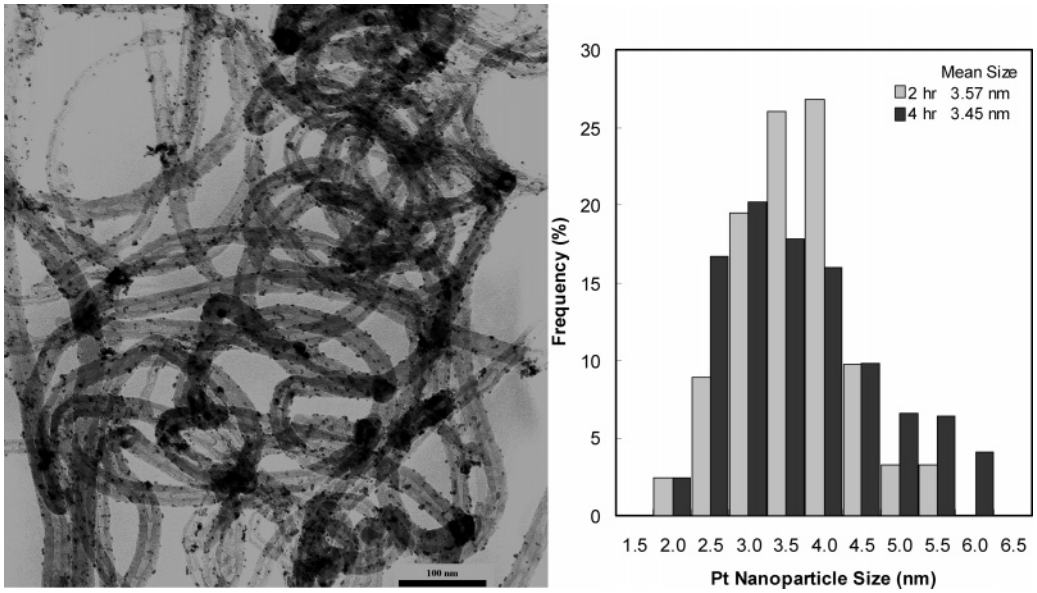

Figure 2. TEM image of 4-h sonochemically treated CNTs followed by Pt nanoparticle deposition. Histogram shows a mean particle size of 3.45 ± 1.02 nm (left panel). Histograms of Pt nanoparticles deposited on the 2- and 4-h treated CNTs are also shown (right panel). The scale bar is 100 nm.

Pt nanoparticles. In examining the D-to-G integrated peak area ratios (Figure 1B), it should be noted that the disordered sp^3 state increases with longer sonochemical treatment. The largest increase occurs between 0 and 1 h of sonication with a plateau being reached at ~2 h. Because the cross sections of the sp^2- and sp^3-hybridized carbon are known to vary greatly,[16] it is difficult to quantify the degree of CNT surface oxidation based upon examination of the disordered versus ordered carbon on the basis of the intensities. The relative Raman D-to-G band intensities (●, left-hand axis) were comparable to previously measured atomic percent mole fractions of oxygen (■, right-hand axis),[11] obtained from normalizing XPS high-resolution energy scans of the O 1s core level with established sensitivity factors[17] (Figure 1B). The Raman D-to-G integrated peak area ratios are in excellent agreement with functional group saturation occurring at ~2 h after sonochemical treatment; a direct correlation is thus shown between the amount of disordered-to-ordered carbon with —COO—/—CO—/—C═O surface density growth. Deposition of the Pt nanoparticles on the 2-h and 4-h CNTs (not shown) did not change the Raman features.

To create a stable Pt—CNT interface, initial surface functionalization of the CNTs was crucial for successfully depositing finely dispersed Pt nanoparticles. Treatment beyond the 2-h sonication appeared to degrade the CNT surface without significant gain in the population of surface oxidized species. These structures that resulted in the 48% increase in electrocatalytic activity, relative to its deposition on Vulcan XC72 carbon black,[10] were readily reproducible. Attempts at depositing finely dispersed, ~4 nm diameter Pt clusters were unsuccessful at the 1- and 8-h sonochemical treatments. In the former case, the CNT surfaces were apparently not sufficiently functionalized to form stable Pt—CNT bonds. In the latter case, oxidation may have resulted in sufficient surface damage to hamper Pt cluster binding on the CNT surface. Pt nanoparticles were observed, however, on the 2- and 4-h treated surfaces. The 2-h sonochemical treatment yielded the best results, readily reproduced from ref 10, having an average cluster diameter of 3.57 ± 0.78 nm at a 20 wt % loading as measured by TEM in terms of the quality of dispersion and lack of nanoparticle aggregation. [The previously published TEM image from ref 10 for the 2-h sonochemically treated CNTs is included in Supporting Information.] Figure 2 (left panel) shows a TEM image and histogram of finely dispersed Pt nanoparticles deposited on the 4-h treated CNTs. The clusters had an average cluster size of 3.45 ± 1.02 nm, approximately the same mean size as those of the 2-h treatment. However, the distribution is skewed toward larger cluster sizes in the 4-h treatment, and they are less uniform than those of the 2-h treatment (Figure 2; right panel) owing to different binding interactions between the two interfaces that we describe more fully in the ATR-IR data below.

The XPS Pt $4f_{7/2}$ core level of the Pt—CNT (prepared using a 2-h sonochemical treatment), referenced to the graphitic C 1s level at a BE = 284.4 eV for the C 1s level,[18,19] had a BE = 71.4 eV. XPS analysis of the Pt—CNT produced with the 4-h sonication was identical to that of the 2-h treatment. This BE indicated that the Pt was predominantly in the metallic (zero) oxidation state (Figure 3).[20—22] XPS signals from the C 1s and O 1s and Pt 4f levels and from no other elements were observed. Normalizing to established sensitivity factors,[17] the atomic percent mole fraction of the Pt was

(16) Banerjee, S.; Hemraj-Benny, T.; Balasubramanian, M.; Fischer, D. A.; Misewich, J. A.; Wong, S. S. *Chem. Commun.* **2004**, 772—773.
(17) Wagner, C. D.; Davis, L. E.; Zeller, M. V.; Taylor, J. A.; Raymond, R. H.; Gale, L. H. *Surf. Interface Anal.* **1981**, *3*, 211—225.
(18) Ago, H.; Kugler, T.; Cacialli, F.; Salaneck, W. R.; Shaffer, M. S. P.; Windle, A. H.; Friend, R. H. *J. Phys. Chem. B* **1999**, *103*, 8116—8121.
(19) Suzuki, S.; Watanabe, Y.; Ogino, T.; Heun, S.; Gregoratti, L.; Barinov, A.; Kaulich, B.; Kiskinova, M. *Phys. Rev. B* **2002**, *66*, 8119—8121.
(20) Delrue, J. P.; Pireaux, J. J.; Caudano, R.; Robert, T.; Hecq, A. *J. Vac. Sci. Technol., A* **1981**, *19*, 257—259.
(21) Fleisch, T. H.; Mains, G. J. *J. Phys. Chem.* **1986**, *90*, 5317—5320.
(22) Fleisch, T. H.; Zajac, G. W.; Schreiner, J. O. *Appl. Surf. Sci.* **1986**, *26*, 488—497.

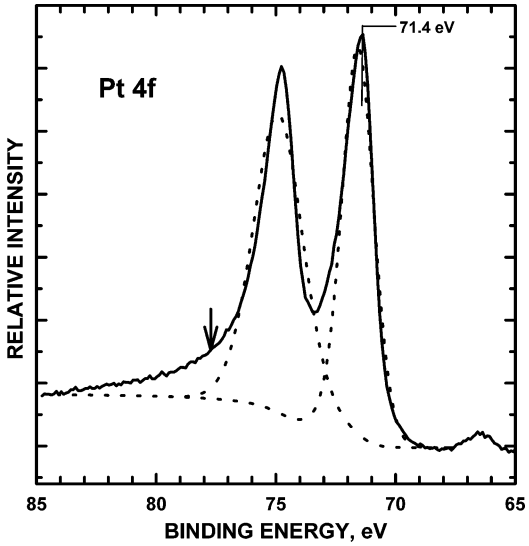

Figure 3. XPS spectrum of the Pt 4f core level after nanoparticle deposition on 2-h sonochemically treated CNTs. Shirley background subtractions were employed; dotted lines denote curve fitting using a 30% Lorenztian−Gaussian line shape. BE peak center of Pt $4f_{7/2}$ orbital = 71.4 eV. Arrow denotes PtO_x.

∼2%. Asymmetry was observed in the $4f_{5/2}$ level at ∼78 eV, which may indicate a small population of PtO or PtO_2,[22,23] which is masked by the much larger signal from metallic Pt. Unfortunately, there was insufficient signal from the Pt oxide (PtO_x) to determine the relative stoichiometric proportions of the PtO and PtO_2 with precision.

To further shed light on this surface structure, EXAFS was performed on the Pt deposited on the 2-h sonochemically treated CNTs to examine the local structure of the nanoparticles. The Pt−CNT samples were examined both as a colloidal suspension in aqueous solution and as a dry powderlike form to get a stronger signal. The density of the Pt−CNT per unit volume was significantly greater as compared to the colloidal suspension, resulting in higher counts. EXAFS is an oscillatory feature in the X-ray absorption above the absorption edge of the target atoms and is defined as the fractional deviation in the absorption coefficient:

$$\chi(k) = \sum \frac{N_j f_j(k) \exp[-2k^2\sigma_j^2]}{kR_j^2} \sin[2kR_j + \delta_j(k)]$$

where R = distance from the target to neighboring atom, N = coordination number of the neighboring atom, and σ^2 is the disorder of the neighbor distance (i.e., the Debye−Waller factor). The photoelectron wavenumber $k = [2m(E - E_0)/\hbar^2]^{1/2}$, $f(k)$ is the scattering amplitude, and $\delta(k)$ is the phase shift.[24] Oscillations arise from the photoelectron wave backscattering from the nearest neighbor atoms. Assuming a cuboctahedron structure, predicted for the Pt nanoparticles of this size (3.5 nm in diameter) deposited on a carbon surface,[25] there are ∼1500 atoms per cluster on the 20% Pt loaded, 2-h sonochemically treated CNT surface. Excluding other effects, a majority of the bonding would emanate from bulk Pt−Pt interactions. However, the EXAFS oscillations point to Pt coordination to lower molecular weight atoms.

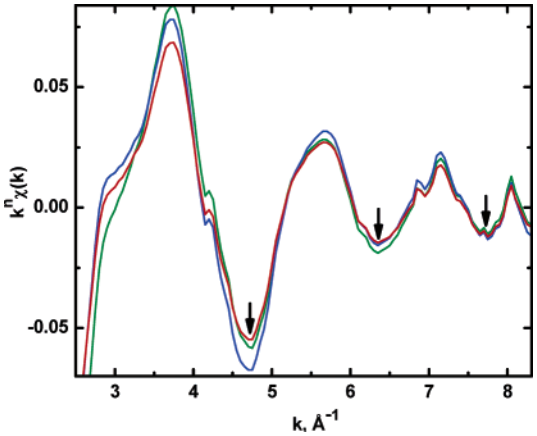

Figure 4. EXAFS oscillations, $k^n\chi(k)$ plotted in k space, of Pt nanoparticles deposited on 2-h sonochemically treated CNTs in dry, powder-like form at k weights n = 1 (blue), 2 (red), and 3 (green). Arrows denote areas of destructive interference.

Table 1. EXAFS Background Removal and Forward FT Parameters

parameter	Pt foil	PtO_2 standard	dry Pt−CNT	aqueous Pt−CNT
edge step, eV	1.231	4.709	3.321	0.039
R_{bkg}, Å	1.25	1.00	0.900	1.00
pre-edge range, eV	−141.80 to −30.00	−91.50 to −65.00	−91.00 to −40.00	−152.02 to −144.81
norm. range, eV	150.00−757.90	150.0−498.99	150.00−699.49	150.00−503.18
k spline range, Å^{-1}	0−15.006	0−12.539	1.493−9.000	0−12.582
E spline range, eV	0−857.932	0−599.031	8.493−308.609	0−603.146
fast FT k weight	2	2	1	1
fast FT k range, Å^{-1}	2−14.95	2−12.65	2.881−8.5	2−12.532

Figure 4 shows the $\chi(k)$ EXAFS oscillations of the dry Pt−CNTs plotted with k weights, n = 1, 2, and 3. Parameters for background subtraction for the dry Pt−CNT sample were identical (Table 1) for all of the generated EXAFS spectra, except for the aforementioned k weightings. In processing the EXAFS data, high k weighting places a higher priority on selecting a spline matching to background at higher k values while lower k weighting has the same effect at lower k values.[26] Contributions to the EXAFS oscillations of low molecular weight neighboring atoms are pronounced at lower k while those of higher molecular weight are pronounced at higher k. Because the k weightings are applied to the same data, if all of the interactions were bulk Pt−Pt (theoretically), there would be no mismatch in the EXAFS oscillations. However, a progressively increasing mismatch of the EXAFS intensities is observed when comparing lower and higher k weights. The degree of mismatch is particularly pronounced where the oscillations destructively interfere, denoted by the

(23) Kim, K. S.; Winograd, N.; Davis, R. E. *J. Am. Chem. Soc.* **1971**, *93*, 6296−6297.
(24) Stern, E. A. Theory of EXAFS. In *X-ray Absorption: Principles, Applications, Techniques of EXAFS, SEXAFS and XANES*; Koningsberger, D. C., Prins, R., Eds.; Wiley and Sons: Eindhoven, 1988; Vol. 92, pp 3−51.
(25) Frenkel, A. I.; Hills, C. W.; Nuzzo, R. G. *J. Phys. Chem. B* **2001**, *105*, 12689−12703.
(26) Sayers, D. E.; Bunker, B. A. Data Analysis. In *X-ray Absorption: Principles, Applications, Techniques of EXAFS, SEXAFS and XANES*; Koningsberger, D. C., Prins, R., Eds.; Wiley and Sons: Eindhoven, 1988; Vol. 92, pp 211−253.

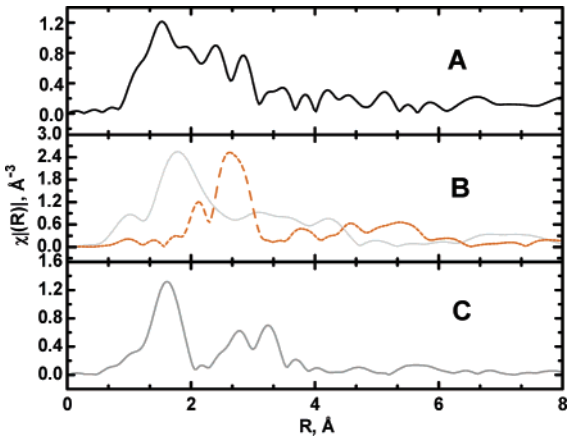

Figure 5. FTs of EXAFS oscillations plotted in *R* space of (A) Pt−CNTs in an aqueous colloidal suspension; (B) Pt−CNTs in dry, powderlike form (solid gray line; a Pt foil scan is shown as a dotted, orange spectral line); and (C) PtO_2 standard. Pt−CNTs prepared from 2-h CNT sonochemical treatment, followed by deposition of Pt nanoparticles.

arrows at the wave troughs (Figure 4). The abscissa coordinates where the mismatches are observed (distances between the highest and lowest troughs in parentheses) are at $k = 7.75$ (0.0024), 6.35 (0.0043), and 4.70 Å^{-1} (0.0126). In comparing the different *k* weights, a greater a mismatch is observed at lower *k*, which is suggestive of Pt bound to a lower molecular weight atom in the local coordination. Fourier transformations (FTs) of the oscillations of this solid Pt−CNT sample into real space were performed and compared with those of the Pt−CNT in colloidal suspension. For further comparison, a FT of a PtO_2 reference sample (magnitudes in *R* space) was plotted (Figure 5). All of the Pt−CNT EXAFS spectra were obtained in the fluorescence mode. No low spline clamp, a strong high spline clamp, and a d$k = 4$ and a Kaiser−Bessel window were used for the FTs. Other parameters used for optimized background removal and the forward FT for each of the three samples are listed in Table 1. Scans of the Pt−CNT were taken as a colloidal suspension to simulate conditions under which it would be used as a DMFC catalyst. The Pt−CNT in colloidal suspension had the poorest signal-to-noise ratio because of the limitations in the decreased sample density (Figure 5A). The FT data show the nearest neighbor to the target at $R = 1.53$ Å, a distance that is too short for the typical 2.77 Å bulk Pt−Pt bond length. To enhance the S/N for EXAFS analysis, the sample was dried to concentrate it prior to placing in the beamline. In the dry Pt−CNT sample, the nearest neighbor distances were still shorter ($R = 1.78$ Å) than predicted for Pt−Pt (Figure 5B). The low *R* value feature at $R = 1.01$ Å is an artifact of imperfect background subtraction due to the intense Pt L_{III} white line at the absorption edge. The FTs of both the dry and the colloidal solution suspended Pt−CNTs seemed to point to Pt low-molecular-weight atom coordination. The dotted-line spectrum is that of the reference foil, obtained in the transmission mode for comparison. The strong peaks between 2 and 3 Å correspond to the interaction occurring between the first nearest neighbor (1NN) Pt atoms. Peak positions of the FT at $R = 2.12$ and 2.70 Å are in good agreement with positions observed by others[25,27] for Pt foil. In comparing *R* values with both those of the colloidal aqueous solution and those of solid Pt−CNT samples, the predominant 1NN interaction in these samples is clearly not with Pt−Pt. The only two low-molecular-weight atoms present that can interact with Pt are C and O. Because the Pt−CNT colloidal solution conditions did not exceed 125 °C during the reduction step to produce the Pt nanoparticles,[10] the formation of PtC in the cluster was unlikely because temperatures in excess of 560 °C are required to form the carbide.[28,29] PtO_2 or PtO is more likely to form than the carbide. A FT of a reference PtO_2 powder is shown in Figure 5C. The location of its 1NN, signifying Pt−O, is seen at $R = 1.59$ Å which closely matches the observed nearest neighbor distance in the colloidal aqueous solution suspended Pt−CNT sample at $R = 1.53$ Å. Evidence points to the presence of PtO_x on the Pt−CNT surface but not in the bulk of the nanoparticles. Because the EXAFS scattering is sensitive only to the first few atomic shells and given the size of the Pt nanoparticles (∼1500 atoms), PtO_x appears to be present only at the topmost surface layers of the cluster. A majority of the Pt atoms are in the metallic (zero) oxidation state, consistent with the observed XPS Pt 4f core level shift.

Although the degree of surface oxidation was readily quantitated in our previous study,[11] spectroscopic peak assignments from −COOH in the XPS could not be unambiguously made as a result of the fact that the C 1s core levels of −COOH overlap with those of −C−OH and −C═O groups,[15,30−32] which were also present. The infrared data (vide infra), however, expands our ability to make these functional group assignments. The ATR-IR difference spectra stackplot of the CNTs (with the raw, untreated nanotubes used as a blank) clearly showed distinct stretches of the (1) −C═O, (2) asymmetric $-COO-_{(as)}$, and (3) symmetric $-COO-_{(s)}$ ester groups from the 1-, 2-, 4-, and 8-h sonochemical treatment times (Figure 6). Hydroxyl stretches on the CNT surface at ∼3150 and 3600 cm^{-1} were also observed (Figure 7; left panel). Key ATR-IR frequencies observed for the sonochemically treated CNTs are summarized in Table 2.

It should be noted that there is a paucity of vibrational data on multiwalled CNTs as most of the literature focuses on single-walled CNT systems; hence, some imprecision is anticipated when making direct comparisons with literature values to date. Intensities on single-walled CNTs, observed between 1300 and 1600 cm^{-1}, are typically left unassigned.[33−35] However, the feature at ∼1400 cm^{-1} can be assigned

(27) Zhang, Y.; Toebes, M. L.; van der Eerden, A.; O'Grady, W. E.; de Jong, K. P.; Koningsberger, D. C. *J. Phys. Chem. B* **2004**, *108*, 18509−18519.
(28) Kojima, I.; Miyazaki, E.; Iwao, Y. *Appl. Surf. Sci.* **1982**, *10*, 27−41.
(29) Lamber, R.; Jaeger, N. I. *Surf. Sci.* **1993**, *289*, 247−254.
(30) Hiura, H.; Ebbesen, T. W.; Tanigaki, K. *Adv. Mater.* **1995**, *7*, 275−276.
(31) Hidefumi, H.; Ebbeson, T. W.; Katsumi, T. *Adv. Mater.* **1995**, *7*, 275−276.
(32) Lee, W. H.; Lee, J. G.; Reucroft, P. J. *Appl. Surf. Sci.* **2001**, *171*, 136−142.
(33) Mawhinney, D. B.; Naumenko, V.; Kuznetsova, A.; Yates, J. T., Jr.; Lui, J.; Smalley, R. E. *J. Am. Chem. Soc.* **2000**, *122*, 2383−2384.
(34) Matranga, C.; Bockrath, B. *J. Phys. Chem. B* **2004**, *108*, 6170−6174.
(35) Feng, X.; Matranga, C.; Vidic, R.; Borguet, E. *J. Phys. Chem. B* **2004**, *108*, 19949−19954.

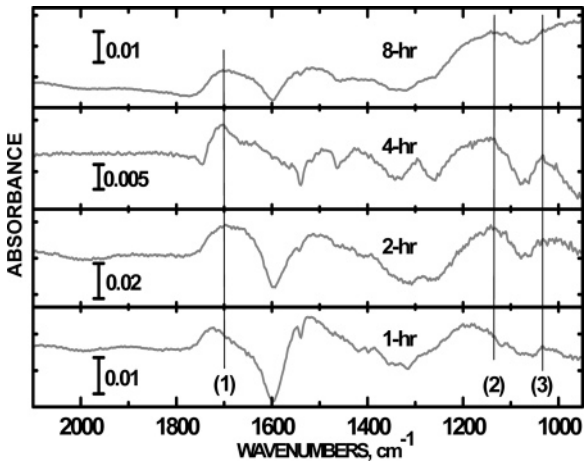

Figure 6. ATR-IR difference spectra of the 2100−900 cm^{-1} region of sonochemically treated CNTs before Pt nanoparticle deposition. Untreated CNTs were used for background subtraction. Features from (1) carbonyl and ester (2) asymmetric and (3) symmetric stretches are observed.

to a C−H bending motion[36,37] on hydrogenated single-walled CNTs. Because we observe accompanying modes at ∼2920 cm^{-1} in our data after 1- and 2-h sonochemical treatments (2916 cm^{-1}) followed by Pt cluster deposition (2920 cm^{-1}, vide infra) near the hydroxyl region (Figure 7; blue trace on right panel), we also make this assignment. Note that these bending modes were not observed in the 2-, 4-, and 8-h treatments because the C−H bend absorbance signal from the more intense OH stretches that accompanied CNT surface oxidation was obscured. In the 2-h, Pt-deposited system, the diminished OH stretch (vide infra) allowed for observation of the C−H bend.

The most pronounced feature development is that of the carbonyl stretch consistent with interaction with an ester group.[38] The peak at 1725 cm^{-1} in the 1-h treated sample grew in and shifted to a lower frequency at 1700 cm^{-1} (peak 1) after a 2-h sonochemical treatment. The shift continued to 1705 cm^{-1} after a 4-h sonochemical treatment; this peak position is predicted for an ester group with increasing conjugation accompanying surface oxidation.[38] The shift to lower frequency is due to increased surface oxidation, which changes the local electronic environment through increased availability for resonances that act to decrease the effective bond order of the carbonyl bond.[39] Overall, the IR peaks shift to lower frequencies as the surface oxidation increases. Note that the frequency stretches are higher for the 4- and 8-h treated samples than for the 2-h sample (Figure 6). This result is consistent with the Raman data (Figure 1) showing CNT surface decomposition with excess sonication time, further validating our previous XPS findings showing that increased sonication decomposes the surface functional groups.[11] Another frequency shift from 1189 cm^{-1} to 1134 cm^{-1} (peak 2) was observed between the 1- and 2-h sonochemical treatments. Also apparent is the intensity development of the $\upsilon(C-O-C)_{as}$ stretch[38] at peak 2 and the $\upsilon(C-O-C)_s$ stretch at 1037 cm^{-1} (peak 3)[33] which grows until reaching a plateau between the 2 and 4 h of treatment before decreasing at 8 h of treatment. We attribute the loss of intensity to degradation of the surface groups (not the CNTs) from over-oxidation. The CNTs, as shown by the Raman data (Figure 5A), retained most of their carbon sp^2 structure from the graphene sheets. Although the peak 2 feature at 1090−1190 cm^{-1} can be assigned to C−O stretching from the CNT surface,[37] it does not indicate a carboxylic acid moiety. The feature falls just outside the expected 1315−1280 cm^{-1} (ref 40) range. The acidic form of COOH has a reported stretch at ∼1735 cm^{-1}, signifying the COOH group tethered onto single-walled CNTs observed by others.[41−43] On multiwalled CNTs, the characteristic stretching frequency has been reported to absorb at 1710 cm^{-1} (ref 44) but was not observed in our data. Also, the carboxylate group has asymmetric $-COO-_{(as)}$ and symmetric $-COO-_{(s)}$ stretches at 1560 and 1400 cm^{-1}, respectively.[42] Neither of these intensities were pronounced in the ATR-IR spectra prior to Pt deposition (Figure 6). The COOH does not seem to be present in appreciable quantities. On the basis of the ATR-IR data, the −COO− species detected in the XPS[11] appears to be attributed to an ester-like species rather than a carboxylic acid. Prior to the deposition of the Pt nanoparticles the CNT surfaces were covered predominantly with −C═O, −COO−, and −C−OH groups. It is with these moieties that the Pt nanoparticles interact and bind. Surface hydroxyls, on the other hand, were prevalent throughout the sonochemical treatments from 1 to 8 h as seen in the stretching region near the ∼3150 cm^{-1} (peak 4) region (Figure 7; left panel). Disordered OH stretching on the CNT surface appeared at 3500−3800 cm^{-1} (peak 5), likely due to weakly bound surface hydroxyls with possible lateral interactions (e.g., H bonding) between them.[45] Peak 4 remains intense throughout the sonication treatment times. Peak 4 broadens and increases in intensity with increased oxidation.[38] Peak 5 begins to develop after 2 h of sonication and then dominates after the 8-h treatment. Although precise quantification of peak 5-to-peak 4 is difficult because of the high background, an increase in the peak 5 intensity with longer sonochemical treatment is observed. The relatively larger peak 5-to-peak 4 peak area ratio at the 8-h sonochemical treatment (Figure 7; left panel) is likely a result of surface over-oxidation that decomposed the surface functional groups prior to nanoparticle deposition. Peak 4 (∼3150 cm^{-1}) is assigned to an ordered OH stretch where the hydroxyl is coordinated to the CNT surface. Peak 5 is assigned to

(36) Khare, B. N.; Meyyappan, M.; Cassell, A. M.; Nguyen, C. V.; Han, J. *Nano Lett.* **2002**, *2*, 73−77.
(37) Ellison, M. D.; Good, A. P.; Kinnaman, C. S.; Padgett, N. E. *J. Phys. Chem. B* **2005**, *109*, 10640−10646.
(38) Smith, A. L. *Applied Infrared Spectroscopy*; Wiley and Sons: New York, 1979.
(39) Drago, R. *Physical Methods for Chemists*, 2nd ed.; Surfside Scientific: Gainesville, FL, 1992.
(40) Colthup, N. B. Infrared spectroscopy. In *Encyclopedia of Physical Science and Technology*, 3rd ed.; Meyers, R. A., Ed.; Academic Press: New York, 2002; Vol. 7, pp 793−816.
(41) Mawhinney, D. B.; Naumenko, V.; Yates, J. T.; Liu, J.; Smalley, R. E. *Chem. Phys. Lett.* **2000**, *321*, 292−296.
(42) Petroski, J.; El-Sayed, M. A. *J. Phys. Chem. A* **2003**, *107*, 8371−8375.
(43) Zhang, J.; Hongling, Z.; Qing, Q.; Yang, Y.; Li, Q.; Liu, Z.; Guo, X.; Du, Z. *J. Phys. Chem. B* **2003**, *107*, 3712−3718.
(44) Kim, B.; Sigmund, W. M. *Langmuir* **2004**, *20*, 8239−8242.
(45) Irish, D. E.; Brooker, M. H. Raman and Infrared Spectral Studies of Electrolytes. In *Advances in Infrared and Raman Spectroscopy*; Clark, R. J. H., Hester, R. E., Eds.; Heyden and Son, Ltd.: London, 1976; Vol. 2, pp 212−311.

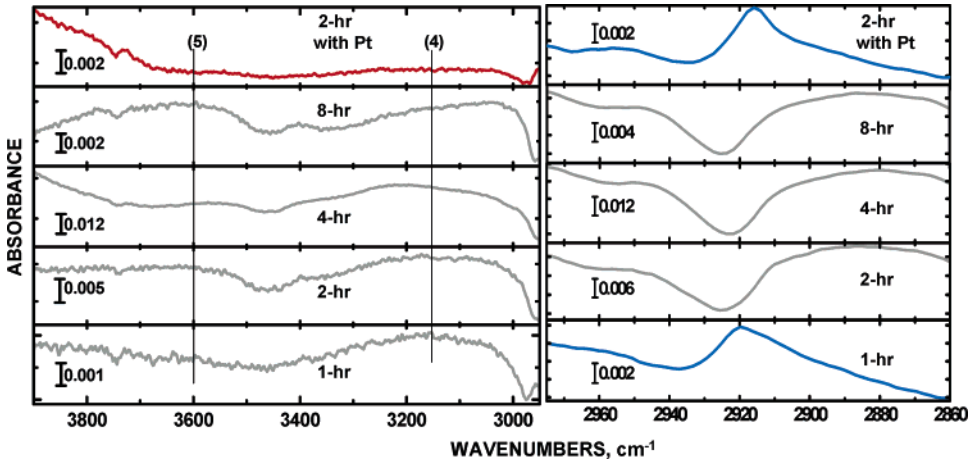

Figure 7. ATR-IR spectra of 3900−2950 cm^{-1} region of sonochemically treated CNTs before Pt nanoparticle deposition. Raw data are shown. Peaks 4 and 5 denote ordered and disordered OH stretches, respectively (left panel). The red trace denotes a reduced signal from OH after Pt nanoparticle deposition. The blue trace denotes stretches from C−H bending modes due to the multiwalled CNT surface (right panel).

Table 2. Vibrational Frequencies of Multiwalled CNTs after Sonochemical Treatment

sonochemical treatment, h	C═O, cm^{-1}	unassigned, cm^{-1}	C−O stretch, cm^{-1}	COO^-, cm^{-1}
1	1725	1510	1191	1033
2	1700	1487	1138	1031
4	1705	1518	1143	1030
8	1700	1520	1133	1028

disordered hydroxyls weakly bound (physisorbed) to the CNT surface. The increase in surface disorder resulted from the breakup of the sp^2-hybridized carbon due to sonication as shown by the Raman data (Figure 1). We attribute the increase in peak 5 (Figure 7; left panel) to the disordered OH groups emanating from over-oxidation of the CNTs.

In the 2- and 8-h samples the O−H stretch of physisorbed water can be seen at ∼3650 cm^{-1}. We attribute the decreased signal of these peaks in the 1- and 4-h treatments to slight variations in drying. Upon Pt nanoparticle deposition, a marked decrease in peaks 4 and 5 (Figure 7; left panel) was observed [the OH stretch greatly diminishes (red trace)] along with a drop in the pH of the supernatant solution in which the Pt nanoparticles were formed. Surface hydroxyls, both in the ordered (∼3150 cm^{-1}) and disordered (∼3600 cm^{-1}) forms, decreased as the Pt nanoparticles were tethered onto the CNTs. Accompanying the disappearance of the OH stretch, a small but measurable drop in pH was observed. The solution pH dropped by [$\Delta(\Delta pH) =$] 0.358 ± 0.037 units before and after the Pt cluster deposition ($n = 3$). Changes in pH before and after deposition were compared with pH changes in control experiments containing the same reagents but without the CNTs; thus, the pH drop we report emanated from proton release of the CNT surface only. As surface protons are given off into solution, the OH vibrational stretches, seen in peaks 4 and 5, greatly diminish, suggestive of strong interaction between the Pt nanoparticles and surface hydroxyl O atoms. We hypothesize a C−O−Pt binding interaction; however, we have been unable to collect data using our experimental setup in the 300 to 600 cm^{-1} frequency range to verify the presence of the anticipated Pt−O stretch.[46] This hypothesized structure therefore remains tentative. The measured drop in pH is a surprising result because (1) protons from hydroxyl groups are not known to be acidic and (2) there is a lack of carboxylic acid surface groups. There is possibly interference from Coulombic effects associated with Pt nanoparticle deposition interfering with an accurate measurement of proton release (via influences of the aqueous ionic environment) into the solution. The effects of the surface point-of-zero charge (PZC) were not investigated and are a subject for future study. Proton release was observed at conditions that are removed from the surface PZC. Regalbuto and co-workers have demonstrated that pH near charged surfaces can be unstable;[47,48] thus, PZC conditions need to be taken into account when elucidating the origin of the proton release.

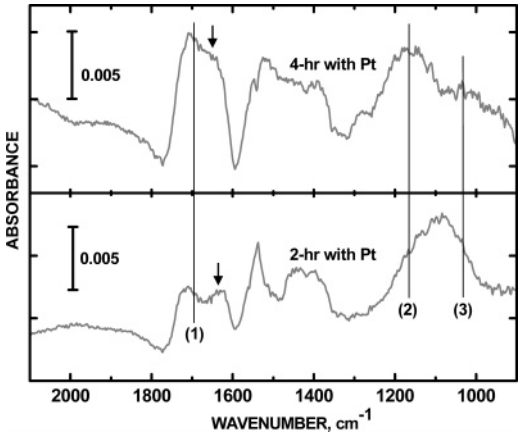

Figure 8. ATR-IR difference spectra of 2100−900 cm^{-1} region of 2- and 4-h sonochemically treated CNTs after Pt nanoparticle deposition. Untreated CNTs were used for background subtraction. Vibrations from (1) carbonyl and ester (2) asymmetric and (3) symmetric stretches as seen in Figure 6 are noted for comparison. Arrows denote a new set of frequencies signifying coordination with Pt nanoparticles.

Figure 8 shows ATR-IR difference spectra of Pt nanoparticles tethered to the 2- and 4-h surfaces. The C−H bending modes at ∼1400 cm^{-1} (Table 3) on both of these

(46) Nakamoto, K. *Infrared and Raman Spectra of Inorganic and Coordination Compounds. Part B: Applications in Coordination Organometallic, and Bioinorganic Chemistry*, 5th ed.; Wiley and Sons: New York, 1997.
(47) Park, J.; Regalbuto, J. R. *J. Colloid Interface Sci.* **1995**, *175*, 239−252.
(48) Hao, X.; Quach, L.; Korah, J.; Spieker, W. A.; Regalbuto, J. R. *J. Mol. Catal. A* **2004**, *219*, 97−107.

Table 3. Vibrational Frequencies of Multiwalled CNTs after Pt Nanoparticle Deposition

sonochemical treatment, h	Scheme 1a, cm^{-1}	Scheme 1b, cm^{-1}	unassigned, cm^{-1}	C—H bend, cm^{-1}	Scheme 1a, cm^{-1}	Scheme 1b, cm^{-1}
2	1712	1629	1536	1399		1092
4	1710	1643	1521	1397	1167	

surfaces further validate the C—H bend (vide supra) assignment (Figure 7; right panel). In comparing the vibrational spectral shifts between the two sonochemical treatments, there appears to be greater Pt binding interactions with the 2-h treated than with the 4-h treated CNT surface. On the 2-h sonochemically treated CNTs with deposited Pt nanoparticles, the C—O ester features, denoted by peaks 2 and 3, become a broad, single band with a center at 1092 cm^{-1}, indicative of strong interaction of the Pt nanoparticles with the ester O. In addition, the carbonyl O band at 1700 cm^{-1} is replaced by two peaks absorbing at 1712 and 1629 cm^{-1} (Tables 2 and 3), indicative of Pt nanoparticle interactions with carbonyl O. On the 4-h treated sample, however, changes in these spectral features were not as pronounced. As the sonochemical treatment ensued, the —C—OH/—COO—/—C═O functional groups may have partially decomposed which thus resulted in poorer binding with the Pt nanoparticles. Pt binding with the carbonyl O was evident from the absorbance shift from a single feature at 1700 cm^{-1} to two peaks at 1712 and 1629 cm^{-1}. Bands from the ester C—O stretches were still present with vibrational stretches at 1160 cm^{-1}. (Compare the frequencies of peak 2 between Figures 6 and 8 for the 4-h treated samples.) A +26 cm^{-1} shift relative to the equivalent stretch was observed on the sonochemically treated CNTs without the Pt nanoparticles. The second C—O feature was still present at 1030 cm^{-1} (peak 3) with the deposited Pt, but the intensity of the absorbance was greatly diminished on the 4-h treated CNT sample. Pt nanoparticles could still be tethered onto the 4-h treated CNTs, albeit more poorly than on the 2-h treated CNTs. In comparing the relative ATR-IR vibrational shifts of the Pt—CNT versus the CNT without Pt on the 4-h treated surface, interactions of Pt with carbonyl O atoms were greater than those with ester O atoms (Figure 8; top spectrum). There were no frequency shifts with peaks 2 and 3, but there was one with peak 1. The poorer Pt—CNT binding on the 4-h sample may likely be due to fewer ester O atoms available for binding to the Pt nanoparticles as compared to the 2-h treatment from over-oxidation due to prolonged surface oxidation. Note that the intensity of the 2-h treatment is four times larger than that of the 4-h treatment (Figure 6). From the 2-h treated samples, it is clear that the Pt loading of the oxidized CNTs dramatically altered the absorbance signal from the C—O stretches in the 1300-to-900 cm^{-1} region (compare Figure 6 with Figure 8, bottom spectrum). The carbonyl C═O signal at 1700 cm^{-1} is less affected, though there is a shift to a higher frequency of 1712 cm^{-1} and the emergence of another stretch at 1629 cm^{-1}, indicative of multiple binding sites for the Pt nanoparticles. This would

Scheme 1. Proposed Pt—CNT Binding Sites

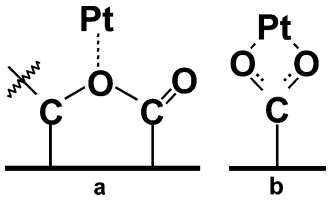

indicate that the Pt coordination is primarily through the C—O species in the 2-h treated CNT samples. Coordination of Pt(II), possibly present in the PtO_x at the perimeter of the nanoclusters (vide supra), has been reported to coordinate with ester O atoms in acidic aqueous media.[49]

On the basis of the ATR-IR data, we propose two possible Pt—CNT surface structures: (1) Pt nanoparticle coordination to ester O atoms bound to the CNT surface, bridging between two carbons and serving as a binding site for the Pt nanoclusters in the form of C(═O)CO(Pt) (Scheme 1a), and (2) attachment via carboxylate ions in which the O atoms effectively have equal bond order and participation the Pt binding in the form of COO(Pt) (Scheme 1b). Features due to structures represented in Scheme 1a,b are simultaneously observed in our data. Tables 2 and 3 summarize the vibrational bands observed before (Figure 6) and after (Figure 8) the Pt nanoparticle deposition onto the multiwalled CNTs. Stretches at ~1700 cm^{-1} signify the C═O stretch prior to nanoparticle binding. The observed blue shift to higher wavenumber (by ~5—10 cm^{-1}) relative to peak 1 for both the 2- and 4-h treatments (Figure 8) upon Pt nanoparticle binding is consistent with coordination of Pt to the ester O atom (Scheme 1a). The pronounced signal at 1167 cm^{-1} from Pt end-on binding to the ester O in the 4-h treated CNT surface (Figure 8; top) is consistent with Scheme 1a and literature reports of transition metal end-on complexation to (M)O—C═O.[50] The coordination formed therein would reduce electron density in the C═O causing this frequency shift. According to Petroski and El-Sayed,[42] because the d band of Pt is close to the Fermi level, electron density to form new bonds will come from the C═O group rather than the Pt. Hence, shifts in the C═O stretch would be sensitive to coordination with Pt. The unassigned frequencies at ~1500 cm^{-1} may be attributed to the C═C structure in the multiwalled CNT. Matranga and Bockrath have noted that these vibrations are close to those of IR active phonons in graphitic carbons associated with single-walled CNTs.[34]

A red shift is observed from ~1160 cm^{-1} (Figure 6) to ~1100 cm^{-1} (Figure 8; bottom) which we attribute to —C—O— binding to Pt due to the fact that Pt nanoparticle deposition resulted in this shift. However, this frequency (at ~1100 cm^{-1}) differs significantly from the anticipated stretch at ~1000 cm^{-1} based on metal—alkoxide frequencies in this region.[46] We speculate that this 100 cm^{-1} difference may be due to Pt—O— interactions with the C═C carbene sheets of the multiwalled CNTs. A corresponding blue shift is observed before and after Pt nanoparticle deposition, from 1487 to 1536 cm^{-1} when Pt was deposited on the 2-h treated

(49) Sen, A.; Lin, M.; Kao, L.-C.; Hutson, A. C. *J. Am. Chem. Soc.* **1992**, *114*, 6385—6392.
(50) Mascetti, J.; Tranquille, M. *J. Phys. Chem.* **1988**, *92*, 2177—2184.

CNTs (Figure 8; Tables 2 and 3) which could result from decreased electron density in the CNT C═C structure upon binding. In addition, a new set of frequencies are observed at ∼1630−1645 cm^{-1} (Table 3) upon Pt nanoparticle deposition, denoted by the arrows in Figure 8. These stretches match with published values for a COO(Pt) coordination[46] depicted in Scheme 1b after Pt nanoparticle deposition (2-h treatment in Figure 8). Furthermore, an accompanying stretch expected at ∼1100 cm^{-1} for the COO(Pt) coordination is also observed in our data at 1092 cm^{-1}.

In summary, solution sonochemical oxidation produced surfaces containing −C−OH, −C═O, −C−O−C−, and −COO− surface groups with little or no COOH present. While most of the Pt in the clusters is present in the metallic form, the outermost surface of the Pt clusters consists of PtO_x. Upon Pt nanoparticle deposition, the finely dispersed clusters bind to the CNTs via bonding with ester and carbonyl O atoms in the form of COO(Pt) and C(═O)CO(Pt), signals of which are observed in our data. These Pt−CNT surface structures appear to be involved in the enhanced electrocatalytic activity observed in the reported DMFC ORR.

Acknowledgment. We gratefully acknowledge the support (in part) of this work from the American Chemical Society Petroleum Research Fund (39542-G2), the Missouri Research Board (1149), the Foundation for Chemical Research, Inc., and the University of Missouri−Rolla Intelligent Systems Center. We thank Prof. Sanju Gupta, Mr. Nathaniel D. Smith, and Mr. Justin Riley of Missouri State University (Springfield, MO) for assistance with the Raman measurements and Prof. Martin Shafer and Mr. Brian Majestic of the University of Wisconsin−Madison for assistance with the PtO_2 reference measurements. We are indebted to Dr. Jeffrey P. Fitts and Mr. Syed Khalid of the Brookhaven National Laboratory and Drs. Shelly D. Kelly and Klaus Attenkoffer of the Argonne National Laboratory for helpful discussions.

Supporting Information Available: TEM image of Pt nanoparticles with a mean size of 3.57 ± 0.78 nm diameter (PDF). This material is available free of charge via the Internet at http://pubs.acs.org.

CM0518978